Mesh convergence study for hydraulic turbine draft-tube

C Devals[1], T C Vu[2], Y Zhang[1], J Dompierre[1], F Guibault[1]

[1] École Polytechnique de Montréal, Montréal, QC, Canada
[2] Andritz Hydro Canada Inc, Pointe-Claire, QC, Canada

Email: christophe.devals@polymtl.ca

Abstract. Computational flow analysis is an essential tool for hydraulic turbine designers. Grid generation is the first step in the flow analysis process. Grid quality and solution accuracy are strongly linked. Even though many studies have addressed the issue of mesh independence, there is still no definitive consensus on mesh best practices, and research on that topic is still needed. This paper presents a mesh convergence study for turbulence flow in hydraulic turbine draft-tubes which represents the most challenging turbine component for CFD predictions. The findings from this parametric study will be incorporated as mesh control rules in an in-house automatic mesh generator for turbine components.

1. Introduction

During the last decade, CFD tools and methodology have evolved tremendously, and now allow performing, on a daily basis, studies with a precision that was unattainable even a few years ago [1]. In this context, computational flow analysis has become an essential tool for hydraulic turbine designers. The first step in the flow analysis process is to create a valid mesh for the computational flow domain and the CFD engineer has to figure out what is the desirable mesh size to get a mesh independent flow solution. But the accuracy of a RANS flow solution does not depend only on the mesh size. There are several parameters governing the mesh generation that influence the final solution, such as the distance of the first near wall point (Y^+ value), the mesh distance expansion factor toward the core flow, the size of the element in core flow for a given flow Reynolds number, element skewness and orthogonality, etc. Even though many studies have addressed the issue of mesh independence, there is still no definitive consensus on mesh best practices, and research on that topic is still needed. As mentioned in [2], different good quality grids can yield quite different flow fields and sometimes important differences in engineering quantities. Establishing the level of precision required for CFD analysis to be at par with laboratory measurements, therefore remains a matter of debate, especially when the full range of operating conditions of the turbine is considered.

This paper presents a mesh convergence study for turbulent flow in hydraulic turbine draft-tubes which represent the most challenging turbine components for CFD predictions. One of the main parameter which controls the mesh density is the element size in core flow and its distribution in spanwise and through flow directions. Also the mesh distance expansion factor from solid walls, which contributes to resolve the viscous flow boundary layer, is another important parameter. The draft-tube flow analysis, through the parametric study, will be performed for a wide range of inlet swirling flow representing turbine operating conditions from part load to full load. Ansys CFX Reynolds Averaged Navier-Stokes (RANS) equations solver using the standard k-epsilon turbulence model will be

performed for all computations. The findings from this study will be incorporated as mesh control rules in an in-house automatic mesh generator for turbine components.

The paper is structured as follows: first, the proposed CFD methodology is briefly introduced, and then the mesh generation approach is presented, along with a study of mesh control parameters and their influence on the CFD solutions. Two test cases of draft-tube loss computation validated with experimental data are then presented and the paper ends with conclusion.

2. Computational Fluid Dynamics setup

All simulations are based on the solution of the incompressible steady-state Navier-Stokes equations.

2.1. Numerical scheme

The commercial software, Ansys CFX 16.1, implementing the standard RANS model using a two-equation k-epsilon turbulence closure model with scalable wall functions was used to perform all computations. All computations were performed using an automatic numerical stability based blended first and second order scheme for the momentum equations, and a first order upwind scheme for the turbulent advection equations. The wall roughness option is kept at smooth wall. At the outlet of the draft-tube, an average constant pressure of 0 Pa is used with a blend factor of 0.05. Turbulence intensity is set to 5% and the length scale is set at $0.005D_{th}$, where D_{th} is the throat diameter. For steady state computations, the convergence criterion was set to $5x10^{-5}$ on the maximum residuals for all primitive variables.

2.2. Operating and inlet swirl conditions

Eleven synthetic axisymmetrical inlet swirling flow profiles, simulating runner exit velocity flow profile at different operating points of the turbine are used. The velocity flow profile varies from co-rotating solid body in part load to contra-rotating nearly free vortex flow in full load condition. The strength of the swirling flow can be quantified as the swirl intensity which is defined as the ratio of the angular momentum flux to the axial momentum flux. In order to match the flow condition in the hydraulic laboratory, the flow Reynolds number is defined as $Re = \rho V D_{th}/\mu = 3 \times 10^6$, where ρ is the density ($kg.m^{-3}$), V the velocity ($m.s^{-1}$) and μ the dynamic viscosity (Pa.s).

2.3. Draft-tube losses

To evaluate the global precision of solutions, losses in the draft-tube are used as a key indicator that can be compared, in terms of precision, with laboratory measurements. The losses are defined by $\left(ptot_{inlet} - p_{outlet} - 0.5\rho V_{outlet}^2\right)/0.5\rho V_{D_{th}}^2$. In the present paper, the draft-tube loss is normalized for imperial flow coefficient Q_{11}=1 and expressed in % of turbine head. The IEC60193 standard suggests that the maximum random uncertainty on efficiency near the optimum should be ±0.1% gh [3]. This uncertainty applies to the efficiency of the whole turbine, and it should therefore be divided over the 4 main turbine components, casing, distributor, runner and draft-tube. For the sake of simplicity, we divide the uncertainty by 4 to obtain ±0.025% for each component. Furthermore, this uncertainty relates to operating condition of all turbine head, for which the imperial speed coefficient Q_{11} may exceed over 3. Since the draft-tube head loss here is normalized for Q_{11}=1, and since losses vary as the square of mass flow, the uncertainty must also be divided by a value of Q_{11} square. For convenience, the standard uncertainty for each component is divided again by 5, to yield a target uncertainty of ±0.005% on draft-tube head losses. This value will be used throughout the present study to assess whether or not observed fluctuations on efficiency are within an acceptable range of uncertainty.

3. Parameter study on mesh convergence

A fully automatic mesh generation tool specifically designed for draft-tube geometries is used to construct all meshes [4]. This meshing tool accepts as an input the external geometry of a draft-tube imported from Andritz in-house design tools, and automatically constructs a thoroughly customized mesh through the specification of only a few parameters by the user. The mesh is based on a single

multi-block structured mesh combining an O-type block structure near all solid walls and a H-type for the inside flow domain. This high level of automation insures consistency of the meshes generated and eases comparison of performance between distinct draft-tube geometries.

Among the parameters used to control the mesh generation process, a single global parameter allows specifying the mesh resolution level for the whole draft-tube. The mesh resolution level thus specifies the mesh expansion factor from the wall and a relative target element size, allowing the number of vertices to vary to ensure a uniform mesh quality, independent of the actual draft-tube dimensions. The mesh generator allows explicitly controlling the distance of the first point near the wall, and the distinct "skin" region thickness (O type mesh) in the near wall region. Geometric laws are used to control the mesh size expansion inside the skin region and to ensure a smooth transition with neighbouring blocks. This distinct control of the mesh in near-wall regions allows maintaining adequate mesh concentration near the boundaries regardless of the overall mesh resolution level chosen.

In the following sub-sections, we would like to present the effect of the overall mesh resolution level as well as the control of skin thickness, mesh expansion factor and element size in core flow on the draft-tube performance.

3.1. *Mesh resolution level*

As mentioned above, the global parameter mesh resolution level indirectly determines the total number of mesh vertices by controlling the mesh expansions factor and the allowed maximum element size in the core flow. In present study, the mesh resolution level parameter varies from 0.02 to 5 allowing the expansion factor varying from 1.3 to 1.05 and the maximum element size varying from $3\%D_{th}$ to $0.05\%D_{th}$. A one pier elbow draft-tube was used as example, and the obtained draft-tube size varies from 140k to 26M vertices. The distances of the first point next to draft-tube and pier solid wall were kept constant for all mesh resolution levels in order to keep an absolute control on the Y^+ value of all mesh density. Table 1 shows the mesh sizes as function of the mesh resolution and figure 1 shows the mesh distribution at the draft-tube inlet and in the through flow direction for three typical mesh resolutions.

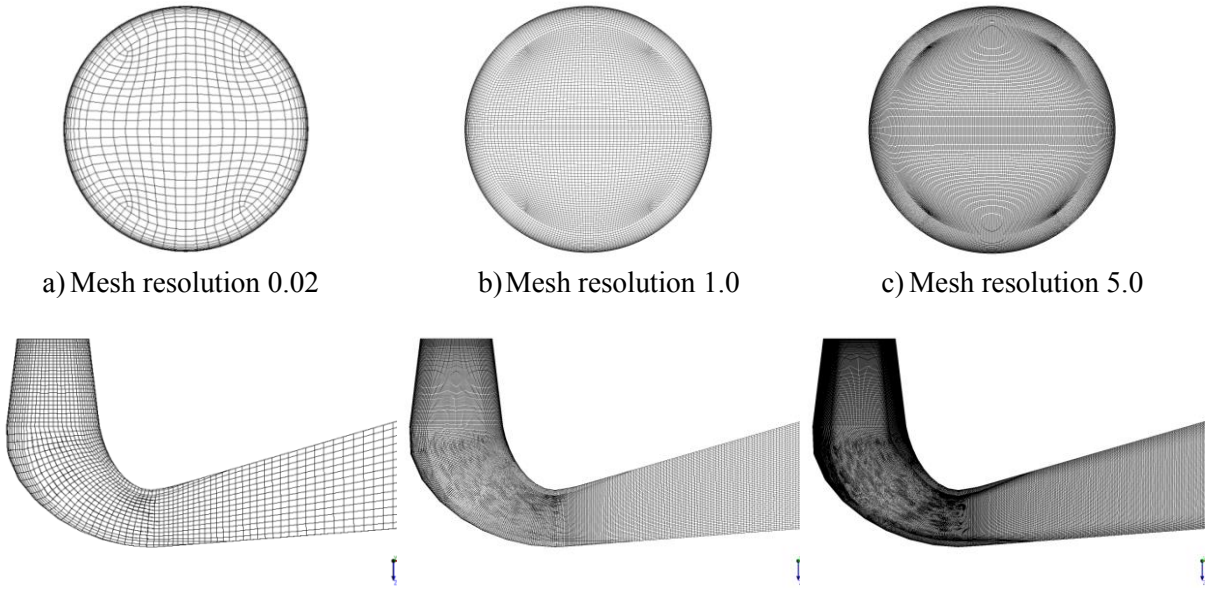

a) Mesh resolution 0.02 b) Mesh resolution 1.0 c) Mesh resolution 5.0

d) Mesh resolution 0.02 e) Mesh resolution 1.0 f) Mesh resolution 5.0

Figure 1. Mesh resolution level for inlet (a to c) and main (d to f)

Table 1. Number of vertices as a function of the mesh resolution level (* indicates reference value).

Resolution	0.02	0.05	0.1	0.2	0.5	1*	3	5
Vertices	0.15M	0.26M	0.45M	0.78M	1.76M	3.53M	12.29M	21.66M

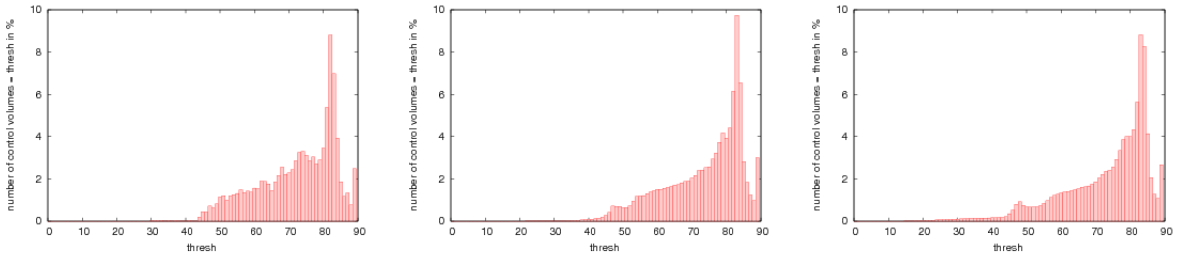

a) Mesh resolution 0.02 b) Mesh resolution 1.0 c) Mesh resolution 5.0

Figure 2. Orthogonality angle

Figure 2 illustrates the distribution of orthogonality angle for three resolution levels. For resolution levels between 0.02 and 1, the orthogonality angle based on CFX post-processing varies between 31 and 21. For resolution levels 3 and 5, the minimum value decreases to 12. CFX recommends an orthogonality factor greater than 20. Poor orthogonality could adversely affect general solution accuracy and robustness [5]. To improve orthogonality of finer meshes, parameters controlling mesh smoothing algorithms could be adjusted, possibly at the expense of robustness of the overall mesh generation process.

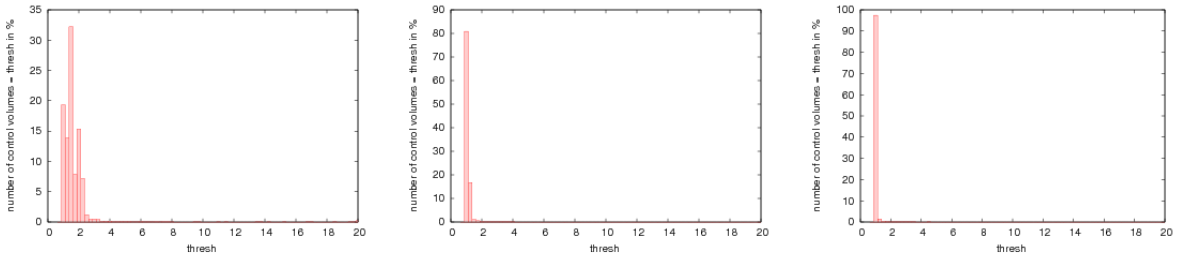

a) Mesh resolution 0.02 b) Mesh resolution 1.0 c) Mesh resolution 5.0

Figure 3. Mesh expansion factor

Figure 3 shows the mesh expansion factor obtained with the post-processing of CFX. It represents the ratio of largest to smallest sector volumes for each control volume and should be less than 20 according to [6]. These figures show the excellent control of the volume expansion of the mesh generator.

Figure 4a shows the normalized draft-tube head loss as a function of the swirl intensity. As expected, the draft-tube loss reaches a minimum at swirl intensity corresponding to the best efficiency point (BEP) and rises rapidly at full load (negative swirl) and at part load. Because of large variations in the draft-tube losses, it is difficult to see the impact of the mesh resolution level in this figure. But the evolution of the draft-tube loss as function of the mesh size is presented separately for three swirl intensities corresponding to full load, BEP and part load in the subsequent figures.

Figure 4b shows the draft-tube loss for different resolution levels varying from 0.02 to 5. The draft-tube losses are normalized by the reference loss value obtained by Richardson's extrapolation [7]. The obtained Richardson's extrapolation loss values are 0.669, 0.222 and 0.950 respectively for full load, BEP and part load. For mesh resolution level 5, the loss values are 0.675, 0.223 and 0.950 respectively. Figures 4c to 4e illustrate the evolution of the draft-tube losses as a function of mesh size for the three typical swirl numbers. The dashed lines indicate a tolerance of ±0.005% around the Richardson extrapolated values. As observed in figures 4d and 4e, solutions with mesh size above 1M vertices fall within the tolerances for BEP and part load, but for full load condition, it requires mesh size higher than 6M for the CFD solution to fall within the tolerances (figure 4c). For the following parameter studies, we use mesh resolution 1 (around 3.5M vertices for one pier DT) as reference value.

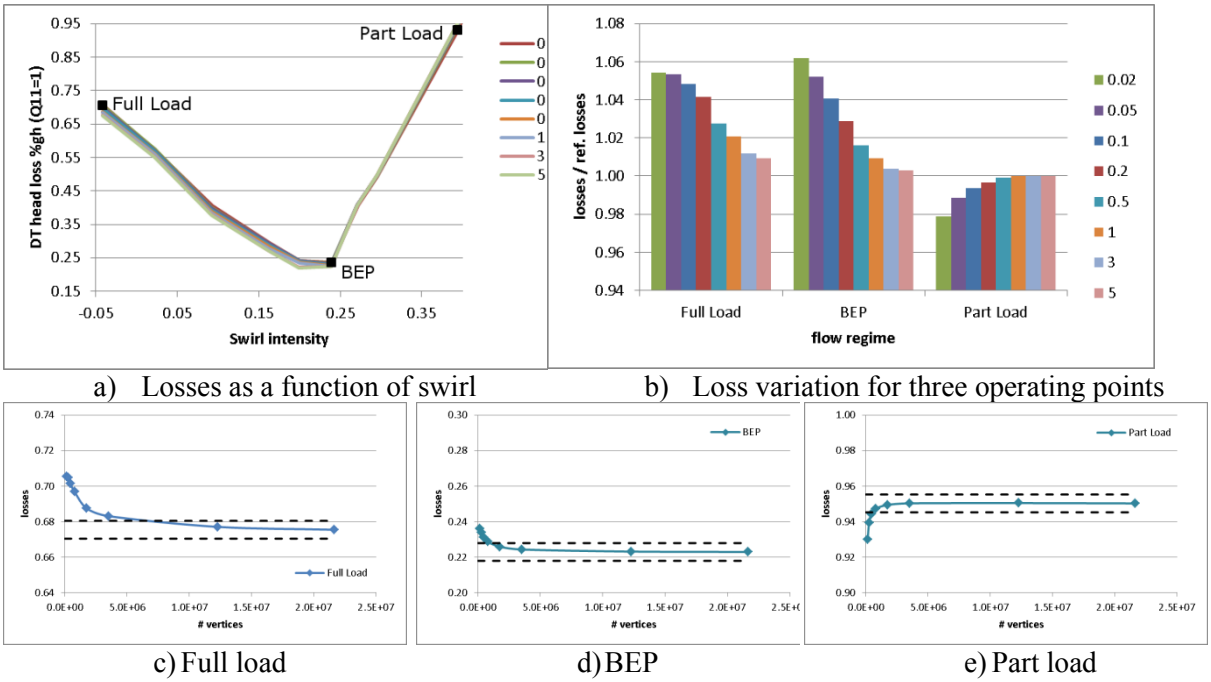

a) Losses as a function of swirl b) Loss variation for three operating points

c) Full load d) BEP e) Part load

Figure 4. Losses for dt A of case 1 as a function of vertices number.

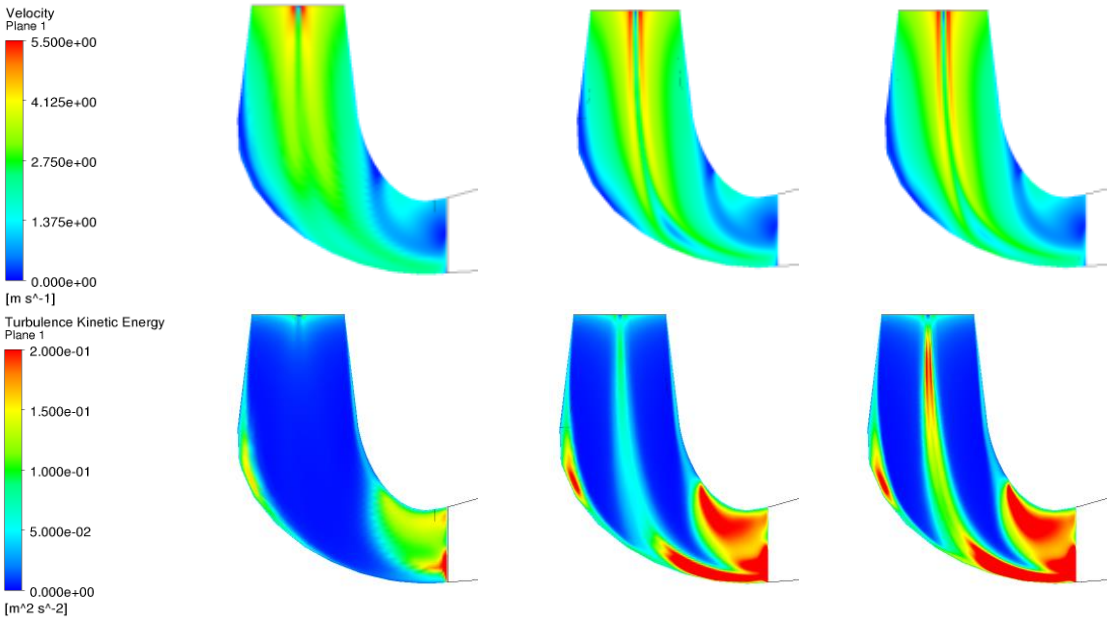

a) Mesh resolution 0.02 b) Mesh resolution 1.0 c) Mesh resolution 5.0

Figure 5. Flow behaviour at full load for case 1

Table 2. Y^+ for BEP and for different mesh resolution level.

	draft-tube wall			pier wall		
resolution	min	ave	max	min	ave	max
0.02	2.0	73	160	2	78	188
1.0	2.5	76	173	2	82	218
5.0	5.0	77	179	2.5	82	223

Figure 5 shows the velocity and the turbulence kinetic energy distribution in the core flow at full load condition with three typical mesh resolutions. While there is not much difference in the velocity

flow behaviour obtained with different mesh size, we notice that the turbulence kinetic energy characteristic is well captured with higher mesh resolution.

As mentioned, near wall boundary meshes are constructed so that mesh distribution be well controlled, regardless of the mesh resolution level. To illustrate this, statistics on Y^+ values are presented in table 2. As may be observed, the average first near wall point distance Y^+ remains constant for all meshes and is around 75. The Y^+ values are within the recommended values (30-300) for computation using wall function [8].

3.2. *Skin thickness*

The effect of the variation of skin thickness near solid wall is studied in this section. Figure 6 shows the mesh distribution for different skin thicknesses varying from 0.06 to 0.12 of D_{th} while keeping constant the mesh expansion factor at 1.15 as reference value. Table 3 shows the number of vertices for its skin thickness which varies from 3.2M to 3.7M vertices.

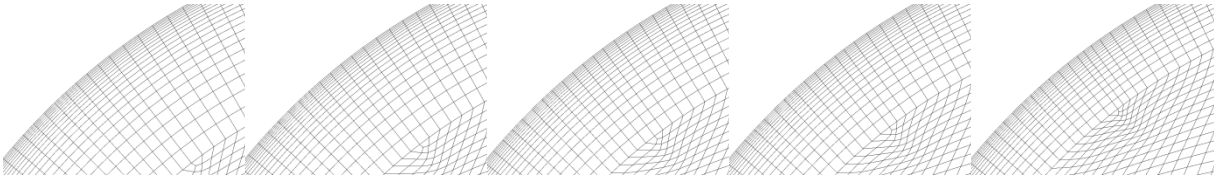

a) 0.12 b) 0.10 c) 0.09* d) 0.08 e) 0.06

Figure 6. Skin thickness

Table 3. Number of vertices as a function of the skin thickness.

Skin thickness	0.12	0.10	0.09*	0.08	0.06
Vertices	3.21M	3.34M	3.53M	3.43M	3.68M

Figure 7 shows the draft-tube losses obtained with different skin thicknesses, normalized by loss values computed using Richardson's extrapolation. This factor is not an important one since the variation of losses is negligible for all flow regimes. The skin thickness does not increase the mesh size so much and this should be the reason of its negligible effect. A value of 0.09 was selected as the reference value for this study.

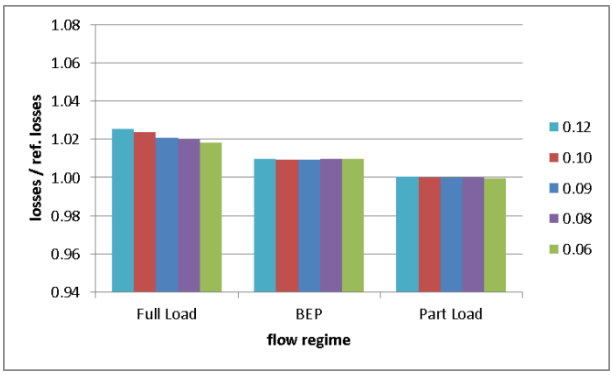

Figure 7. Normalized losses for three flow regimes and different skin thickness values

3.3. *Expansion factor*

The variation of the expansion factor in the skin layer is studied in this section. Figure 8 shows the meshes generated with mesh resolution 1 but for different expansion factors varying from 1.05 to 1.30. In this case the skin thickness stays at $0.09D_{th}$. Table 4 shows the number of vertices for the five distinct expansion factors which varies from 2.1M to 5.7M.

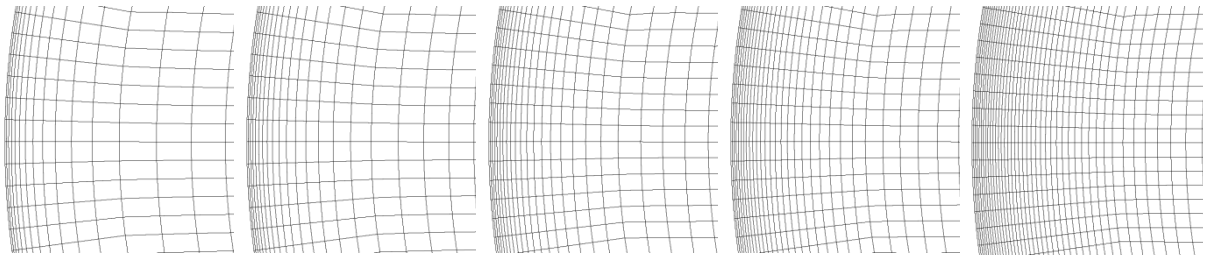

a) 1.30 b) 1.20 c) 1.15 d) 1.10 e) 1.05

Figure 8. Expansion factor

Table 4. Number of vertices as a function of the expansion factor.

Expansion factor	1.30	1.20	1.15*	1.10	1.05
Vertices	2.15M	3.07M	3.53M	4.07M	5.65M

Figure 9 shows the normalized losses (i.e.: losses of the current mesh compared to the Richardson's extrapolation loss values) for three different operating points: full load, best efficiency point and part load.

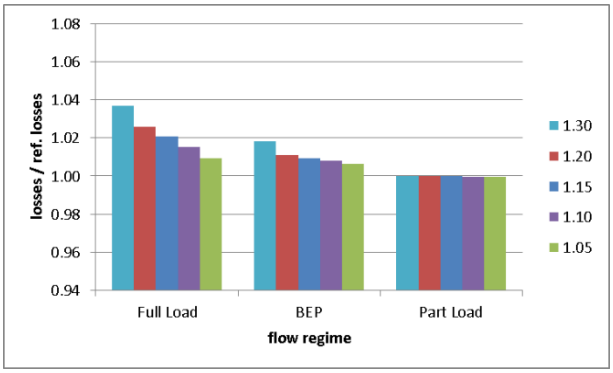

Figure 9. Normalized losses for three flow regimes and different expansion factors

The variation of the expansion factor does not have a significant effect for part load condition and a small effect for the BEP except for the expansion factor equal to 1.3. The effect of the expansion factor variation appears to be more pronounced for the full load case. The losses increase with the increase of the expansion factor in a range of 0.9% to +3.7%. As mentioned in [9-10], the expansion factor should not been greater than 1.25.

3.4. *Maximum element size*

The variation of the allowed maximum element size in the core of the draft-tube is studied in this last section. Figure 10 shows meshes for different maximum element sizes varying from $0.03D_{th}$ to $0.005D_{th}$. Table 5 shows the number of vertices for this factor which varies from 2.6M to 7.2M vertices.

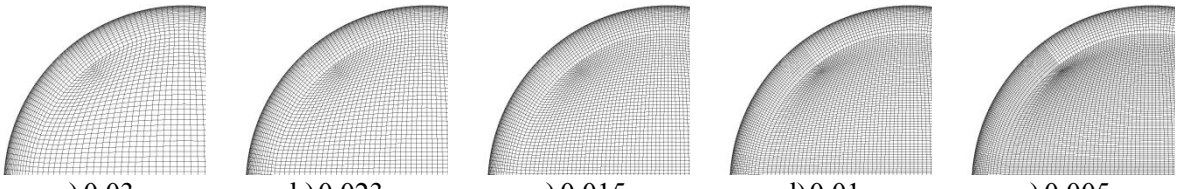

a) 0.03 b) 0.023 c) 0.015 d) 0.01 e) 0.005

Figure 10. Maximum element size

Table 5. Number of vertices as a function of the maximum element size.

Max. Element Size	0.03	0.023*	0.015	0.01	0.005
Vertices	2.67M	3.53M	4.60M	5.82M	7.25M

Figure 11 shows the normalized losses for three operating points (full load, BEP and part load) for different maximum element sizes. Although the mesh size increases by 172%, the maximum difference is around 2.7% compared to the Richardson's extrapolation loss values.

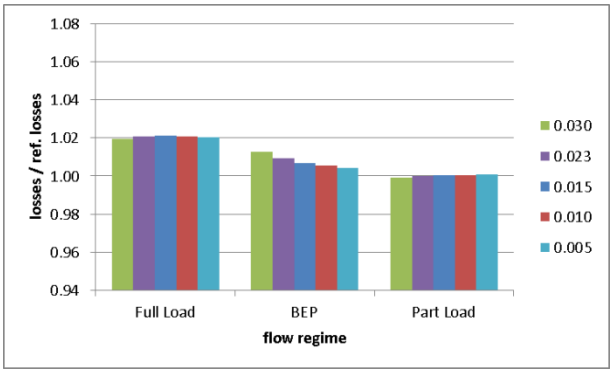

Figure 11. Normalized losses for three flow regimes and different maximum element size values

4. Case study

In the previous section, the mesh convergence study was based on the draft-tube loss absolute values in comparison with the Richardson extrapolation value and on the assumption of uncertainty criteria of ±0.005%. In this study, CFD analyses are performed for two variations of draft-tubes measured in the same assembly with a whole range of mesh resolution levels. The relative performance comparison of the two geometries is then compared against experimental data obtained from the hydraulic laboratory.

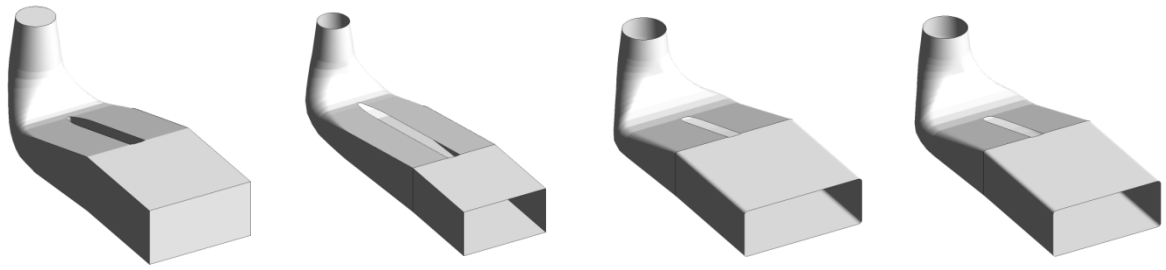

a) Case 1 - dt A b) Case 1 - dt B c) Case 2- dt A d) Case 2 - dt B

Figure 12. Geometries of case 1 (a-b) and case 2 (c-d)

4.1. *Test case 1*

In test case 1, the original draft-tube dt A and the second draft-tube dt B are shown in figure 12a and 12b respectively. Figure 13a shows the efficiency curves obtained from tests for the two draft-tubes equipped with the same upstream components. The comparison between the two gives the gain obtained between the draft-tubes A and B. It indicates that the two draft-tubes have similar performance in the region of the BEP, but dt B performs better at part and full load conditions. The CFD result as shown in figure 13b predicts exactly the same performance trend for all operating conditions, good improvement at full load and part load, and a very small improvement at BEP.

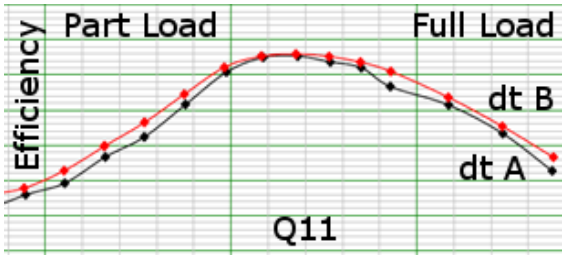

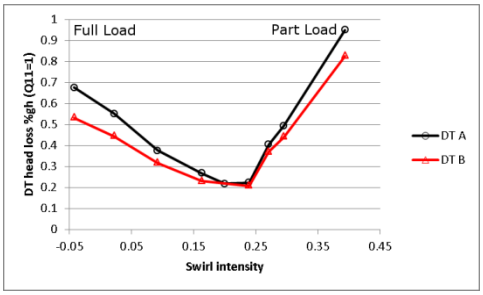

Figure 13. a) Turbine efficiency curves b) Losses of dt A and dt B

The evolution of delta head losses between the two geometries obtained with all mesh resolution levels is shown in figures 14. The plot allows determining a satisfactory level of mesh resolution for mesh convergence. For all three typical inlet swirl conditions, it appears that a mesh resolution level of 0.5 yielding about 1.8M vertices is satisfactory for the uncertainty criteria of *±0.005%*.

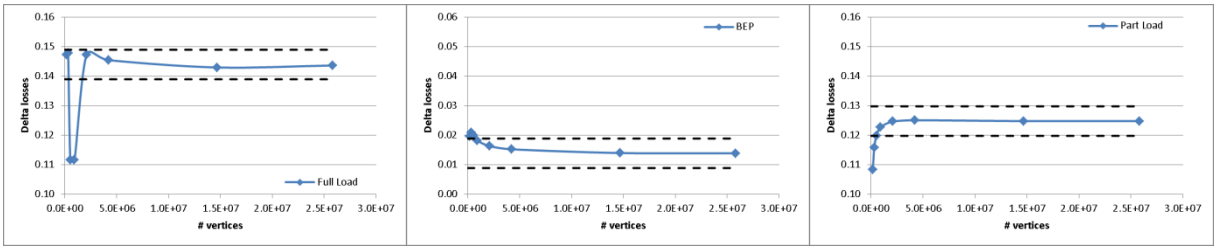

a) Full load b) BEP c) Part load

Figure 14. Difference of losses between dt A and dt B of case 1 as a function of vertices number.

4.2. *Test case 2*

In test case 2, the initial draft-tube dt A and the second draft-tube dt B are shown in figure 12c and 12d respectively. The experimental efficiency curves obtained from the two geometries, as shown in figure 15a, indicate that the second geometry dt B performs much better in full load conditions starting from the BEP but shows no improvement at part load conditions. The numerical performances obtained for the two geometries, as shown in figure 15b, have the same tendency as the experimental data.

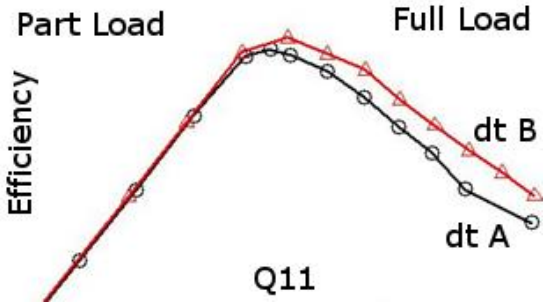

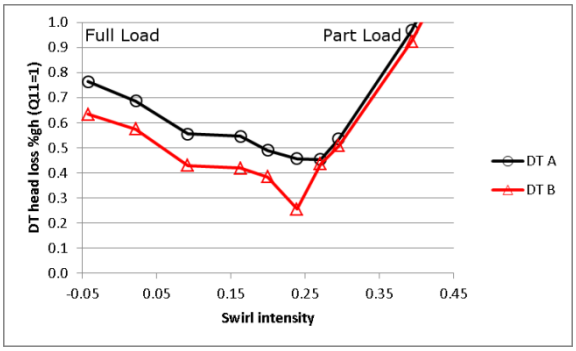

Figure 15. a) Turbine efficiency curves b) Losses of dt A and dt B

As in figure 14, figure 16 represents the evolution of the delta losses between dt A and dt B as a function of number of mesh vertices. Contrary to test case 1, the initial draft-tube dt A of case 2 exhibited very bad flow behaviour when operated at full load, making the analysis of this initial geometry more difficult. Nevertheless, the loss differences obtained for mesh resolution levels above 1 (about 3.5M vertices) fall within tolerances for all three operating conditions.

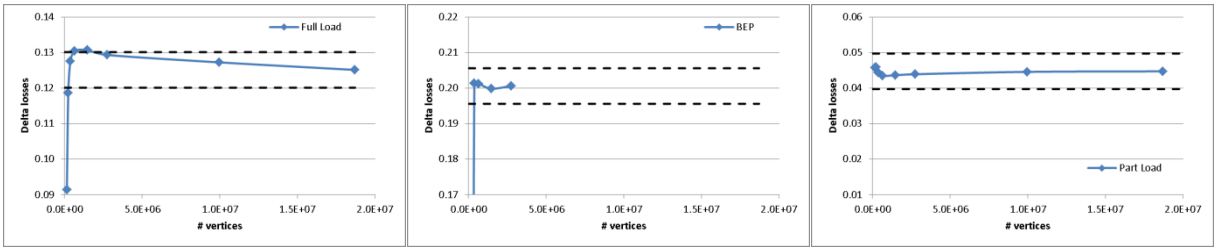

a) Full load b) BEP c) Part load

Figure 16. Difference of losses between dt A and dt B for case 2 as a function of vertices number

5. Conclusion

This paper has presented a mesh convergence study for turbulence flow in hydraulic turbine draft-tubes. Several parameters have been considered such as mesh distance expansion factor from solid wall, skin thickness, maximum mesh size in core flow as well as the mesh resolution level. The mesh convergence study was performed, by mean of draft-tube flow analysis, through a wide range of inlet swirling flows representing turbine operating conditions at model scale from part load to full load. Performing flow analysis with k-epsilon model using wall function, with a strict control of the constant Y^+ and mesh expansion factor from solid wall, an acceptable mesh convergence could be reached with mesh size beyond 4M vertices. The mesh convergence is easier to reach for BEP or at part load condition.

The skin thickness factor has little effect on the draft-tube loss and the element size factor in the core flow has some effects for full load and BEP, but not for part load conditions. The choice of the mesh expansion factor from solid wall is an important parameter. These validations have helped develop a series of meshing guidelines implemented in Andritz Hydro in-house mesh generator that provides consistent loss evaluation results usable for design.

References

[1] Vu TC and Retieb S 2002 Accuracy Assessment of Current CFD Tools to Predict Hydraulic Turbine Efficiency Hill Char. *21th IAHR Symposium on Hydraulic Machinery and Systems* (September 9-12, 2002. Lausanne, Switzerland)

[2] Magnan R, Cupillard S, Gauthier G, Giroux AM, Page M and Deschênes C 2014 Challenges in assessing the grid sensitivity of hydro-turbine CFD simulations. *27th IAHR Symposium on Hydraulic Machinery and Systems* (September 22-26, 2014. Montreal, Canada)

[3] IEC 60193, Hydraulic turbines, storage pump and pump-turbines –Model acceptance tests 1999, Second Edition

[4] Guibault F, Zhang Y, Dompierre J and Vu TC 2006 Robust and Automatic CAD-based Structured Mesh Generation for Hydraulic Turbine Component Optimization *23rd IAHR Symposium on Hydraulic Machinery and Systems* (October 17-21, 2006. Yokohama, Japan)

[5] ANSYS CFX Modeling Guide, Release 16.0, section 15.3.2.1

[6] ANSYS CFX Modeling Guide, Release 16.0, section 15.3.2.2

[7] Richardson L. F. and Gaunt J. A. 1927 The deferred approach to the limit. Part I. Single lattice. Part II. Interpenetrating lattices. *Philosophical Transactions of the Royal Society of London. Series A* **226** 299-361

[8] ANSYS CFX Theory Guide, Release 16.0, section 2.8.1.1

[9] Guénette V 2013 Prédiction numérique de l'écoulement turbulent au sein d'une turbine bulbe par des simulations RANS, Master thesis, Laval University

[10] CFD Online, 2016 Best practice guidelines for turbomachinery CFD, Available at http://www.cfd-online.com/Wiki/Best_practice_guidelines_for_turbomachinery_CFD